Research Square

Preprints are preliminary reports that have not undergone peer review.
They should not be considered conclusive, used to inform clinical practice,
or referenced by the media as validated information.

Implications of weaving pattern on the material properties of two-dimensional molecularly woven fabrics

Liang Zhang

zhangliang@chem.ecnu.edu.cn

East China Normal University https://orcid.org/0000-0001-8605-8681

Xiao He

Shanghai Frontiers Science Center of Molecule Intelligent Syntheses, School of Chemistry and Molecular Engineering, East China Normal University https://orcid.org/0000-0002-4199-8175

Zhi-Hui Zhang

East China Normal University

Yijing Chen

East China Normal University

Shiwei Chen

East China Normal University

Jinrong Yang

East China Normal University https://orcid.org/0000-0002-7678-0360

yun Li

East China Normal University

Article

Keywords:

Posted Date: October 9th, 2024

DOI: https://doi.org/10.21203/rs.3.rs-5148877/v1

License: This work is licensed under a Creative Commons Attribution 4.0 International License.
Read Full License

Additional Declarations: There is **NO** Competing Interest.

Implications of weaving pattern on the material properties of two-dimensional molecularly woven fabrics

Shiwei Chen,[1] Zhi-Hui Zhang,[1] Yuntao Li,[1] Yijing Chen,[1] Jinrong Yang,[1,*] Xiao He,[1,2,,3,*] Liang Zhang[1,2,*]

1. Shanghai Engineering Research Center of Molecular Therapeutics and New Drug Development, Shanghai Frontiers Science Center of Molecule Intelligent Syntheses, School of Chemistry and Molecular Engineering, East China Normal University, 3663 North Zhongshan Rd., Shanghai 200062, P. R. China.

2. Chongqing Key Laboratory of Precision Optics, Chongqing Institute of East China Normal University, Chongqing 401120, P. R. China.

3. New York University-East China Normal University Center for Computational Chemistry, New York University Shanghai, Shanghai, 200062, P. R. China.

E-Mail: jryang@chem.ecnu.edu.cn; xiaohe@phy.ecnu.edu.cn; zhangliang@chem.ecnu.edu.cn

Abstract

Similar to macroscopic woven fabrics, molecularly woven polymers constructed from identical molecular strands but different weaving architectures are anticipated to display diverse physical and mechanical characteristics. Nonetheless, identifying these distinctions and comprehending the underlying mechanisms poses a significant challenge. Herein, we evaluate the impacts of different weaving patterns—plain, mix, and basket—on the characteristics of two-dimensional (2D) organic woven polymers through systematic all-atom simulation. Three weaves, consisting of the same molecular strands, are produced by adjusting the connections of the enantiomers of an inherently chiral 2×2 interwoven grid. Among the tested patterns, the plain weave exhibits superior stability, minimal structural deformation, and the most consistent pore size compared to others. The maintenance of the weaves in kinetically stable high-energy states is attributed to both aromatic stacking and hydrogen bonding interactions between warp and weft strands, while the alteration of weaving patterns leads to variations in the type and strength of these weak interactions. Despite the differences on the weaving pattern, the mechanical stress tends to localize at the contact field. Further analysis on impact resistance and in-plane stretchability highlights how weaving architectures influence the energy dissipation pathways and reinforce the mechanical properties of individual molecular chains. Simulation outcomes indicate that the disparities resulting from various

weave patterns primarily stem from the total number and density of entanglements, as well as the interstrand non-covalent interactions. This research highlights the critical influence of weaving architecture on molecularly interlacing material properties, providing valuable insights for future invention and engineering of molecular-level weaving.

Introduction

Weaving is recognized as one of the most enduring and effective techniques for crafting intricate, ordered materials with properties that fundamentally diverge from those of unorganized components.[1] The weaving of fibers into a fabric structure enhances strength and stiffness to a degree that significantly surpasses that of individual strands, making the woven fabrics highly suitable materials for both military and civil protective applications.[2] Among various woven factors, such as fibril materials, areal mass and projectile sizes, that can influence the mechanical performance of fabrics,[3,4] the modulation of weaving pattern[5,6] is identified as one of the most efficient approaches to balance the strength, stiffness and toughness. Both experimental program and mesoscale numerical models validate this low-cost manufacturing process impacts the flexibility, durability and impact resistance of macroscopic fabrics by altering the mechanisms of energy absorption and dissipation.[7,8]

Unlike macroscopic conventional textiles with well-established manufacturing processes, the construction of 2D or 3D molecularly woven materials with long-range ordered entanglements by from crystalline interlacing 1D flexible molecular strands presents a significant challenge.[9-12] Expanding on the initial concept of 'true' molecular weaving proposed by Busch and Hubin in 2000,[13] creation of organic woven polymers has been achieved on several occasions by using reticular chemistry,[14-16] supramolecular self-assembly,[17-19] surface-templated MOF[20] and tessellation[21] of pre-woven building blocks.[22-26] The obtained polymers exhibit not only expected mechanical properties, but also act as nets for adaptive guest inclusion[27] and fishing ions[21] or template polymer entanglements[28]. Moreover, the few developed approaches with limited availability of chemical components hinders the precise adjustment of the characteristics of molecularly woven textiles. As a result, the performance of such materials is markedly inferior to that of conventional polymers. Therefore, it appears that these interlaced molecular networks are becoming increasingly accessible through synthesis, understanding the structure-property relationship and manipulating material characteristics through molecular engineering of woven factors, akin to what has been achieved in commercial textiles,[5,6] remains undiscovered.

In contrast to weaving fibers on a millimeter scale, molecular weaves are kinetically stabilized in a high-energy state by ordered entanglements and interstrand interactions.[29-33] It is reasonable to infer that the properties of woven polymers with identical chemical composition could be attributed to the total number of entanglements. The preceding simulation on entangled polymers further verifies that rheological[34] and mechanical characteristics[29,35] can be influenced by topological entanglements, which impose physical restrictions on strand movement through the contact field.[36-39] Therefore, we envisage that the modulation of weaving patterns at molecular level, which dictates the density of entanglements in the woven network, should bring similar consequences to that of the macroscopic weaves. Experimental realization of the effects of weaving architectures is currently challenging due to the lack of suitable chemistry capable of linking selected tangles with the required connectivity. Instead, we herein present an all-atom theoretical investigation, exploring the implications of three different weaving patterns (Fig. 1) on the physical and mechanical characteristics of two-dimensional molecularly woven fabrics.

Results and Discussion

Construction of woven fabrics with different patterns.

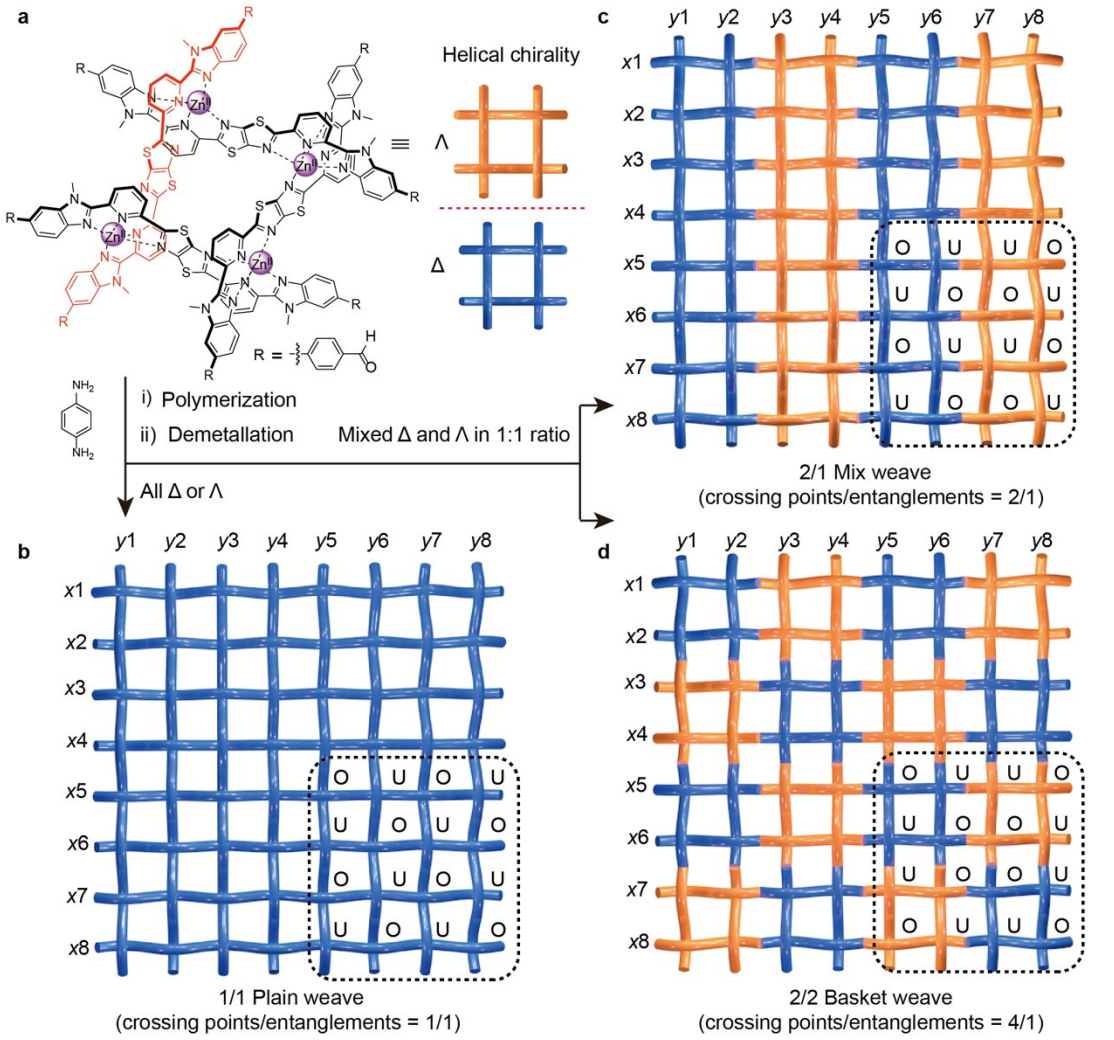


Fig. 1 | Cartoon illustrations showcase three different weaves, all with identical chemical compositions, made from a molecular 2×2 grid repeating unit. (**a**) Chemdraw and schematic depiction of the repeating unit (a 2×2 molecular grid) used to generate the initial models (IS) of three weaving patterns through imine-polymerization and demetallation processes. Due to the inherent helical chirality (Δ and Λ) of the grid, altering the ratio and connectivity of its two enantiomers results in the creation of three designed weaves; (**b**) 1/1 Plain weave consists of enantiopure chiral grids, generating -over-under-over-under- (-O-U-O-U-) sequence in both warp and weft directions; (**c**) 2/1 Mix weave: Two warp threads cross over one weft thread, creating an alternating sequence of over-under-under-over (-O-U-U-O-) along the weft and under-over-over-under (-O-U-O-U-) along the warp; (**d**) 2/2 Basket weave: Two warp threads interlace with two weft ribs as a group, resulting in an -over-under-under-over- (-O-U-U-O-) sequence in both directions. Throughout the simulations, the weft (horizontal) direction is defined as the *x*-axis, and the warp (vertical) direction is represented by the *y*-axis, with crossing points denoting locations where weft and warp threads overlap. Our models comprise 100 grids arranged in a 10×10 array, resulting in a

total of 400 crossing points. A crossing point is deemed a genuine entanglement only when the movement of the strand is mechanically impeded by its neighboring strands. As a result, the three weaves exhibit different entanglement densities (400 in plain weave, 200 in mixed weave, and 100 in basket weave), directly determined by the patterns.

To investigate the influence of weaving patterns on fabric dynamics and mechanical properties without regard to the chemical composition, a Leigh's molecular 2×2 bis(benzimidazolylpyridyl)thiazolo[5,4-d]thiazole (TTZ) grid[40] featuring a planner geometry and inherent helical chirality was choose as the repeating unit for the construction of different woven polymers. The isopentyl groups on the benzimidazole units are replaced by methyl to simplify the model. Terminal aldehyde groups are introduced to facilitate desired network formation through imine condensation with 1,4-benzenediamine linkers (Fig**.** 1a).[41]

Three weaves, namely 1/1 plain weave (Fig. 1b); 2/1 mix weave (Fig. 1c) and 2/2 basket weave (Fig. 1d), are made up of 100 grids in a 10×10 array via a bottom-up strategy. In the plain weave, grids of single-handedness were linked, with horizontal weft threads alternating over and under vertical warp threads, creating a checkerboard-like pattern. Conversely, each grid connected to four neighboring grids with opposite handedness, resulting in two warp threads alternately interlacing with two weft ribs, forming an over-over-under-under (O-O-U-U) crossing arrangement in both directions in the basket weave. In the mix weave, each grid is associated with two neighboring grids of opposite chirality in the warp direction while connected to the grids with the same handedness in the weft orientation, giving an O-O-U-U and O-U-O-U crossing sequences along the weft and warp threads, respectively.

According to our established models, each of the three weaves comprises twenty weft threads intersected by twenty warp threads, resulting in a combined total of 400 crossing points. However, a crossing point is recognized as a genuine entanglement only when the movement of the strand is mechanically impeded by its neighboring strands.[9,38] For instance, in both the 2/1 mixed weave and the 2/2 basket weave, the four crossing points featuring the over-over-under-under (O-O-U-U) pattern are counted as two valid entanglements. Although all weaves possess identical chemical compositions, the total number and density of entanglements (400 in plain weave, 200 in mixed weave and 100 in basket weave) vary directly with the weaving pattern. We envisage that these differences would directly impact the dynamics and mechanical properties of the woven polymers.

Dynamics, Kinetics and Stability of woven fabrics.

Examination of the root-mean-square deviation (RMSD) values (Fig. 2a and Supplementary Information, Figure S1) acquired over a temperature span from 300 to 400 K provides insights into the stability of various woven polymers at equilibrium state (ES). The existence of densely-packed entanglements hampers the dissociation of strands, maintaining all three weaves kinetically stable for the time scale of the calculations, even under ambient temperature conditions.

At 300 K, the plain weave displays the smallest RMSD value, with an average oscillation factor of 0.38 nm. Following closely, the mixed weave and the basket weave exhibit values of 0.46 nm and 0.5 nm, respectively. Despite changes up to 400 K, the RMSD values for the plain weave demonstrate minimal oscillation, indicating exceptional stability. Conversely, notably elevated RMSD values at higher temperatures suggest a progressive decrease in stability for the other two weaves. The mixed weave maintains comparable resistance between 320 K and 380 K, with the RMSD value in the range of 0.5-0.6 nm, while the RMSD value of the basket weave increases to 0.78 nm at 380 K. These results highlight the direct correlation between the stability of woven fabrics and their patterns, with the weave possessing the highest entanglement density exhibiting superior stability (The schematic representation of changes of plain weave, mixed weave, and basket weave at different temperatures were shown in Figure S2-S4). Consequently, the stability of the three weaves can be ranked as follows: 1/1 plain weave, 2/1 mixed weave, and 2/2 basket weave.

Stability variance can also be assessed through measuring the crossing displacement (CD) of all 400 crossings in various weaves from the initial model (IS) to its equilibrium state (ES) (Fig. 2b, Box 1b). Given that all crossing points are regarded as real entanglements in the plain weave, it exhibits the narrowest CD distribution, spanning from 0.1-0.6 nm, with a prominent peak at 0.3 nm. As the entanglement density decreases in the mixed weave, half of the crossing points are no longer directly constrained at their initial positions. This results in a broader distribution of crossing displacement (CD) populations, with the strongest peak shifting to 0.35 nm. The basket weave, featuring the lowest entanglement density, exhibits the widest CD distribution, characterized by two peaks at 0.35 nm and 0.5 nm, respectively. The CD of local crossings on three selected wefts and warps yarns ($y1$, $y4$, $y7$ wrap strands and $x1$, $x4$, and $x7$ weft strands) is also evaluated (Supplementary Information, Figure S6), revealing very similar distribution profiles compared to the global calculation. Several minor peaks appearing in the 1 to 2.5 nm region are attributed to increasing background noise

resulting from the reduction in the number of crossings from 400 to 60.

With the alteration of weaving patterns, we anticipate that the space field (Box 1a) between the warp and weft strands will also be affected. Changes in the space field can not only reflect the flexibility of the weaves but also determine the ability of the molecular fabric to function as a net. Consequently, we analyze the pore size distribution (PSD, Box 1b) using PoreBlazer[42] to assess the degree of deformation between the IS and ES (Fig. 2c). Initially, all three weaving models exhibit similar pore distributions, characterized by three distinct peaks at 0.7, 2.4, and 2.6 nm, suggesting the similarity between their initial models. Upon reaching equilibrium, the plain weave demonstrates the least variation in the space field, evident from the presence of two peaks at 2.7 and 2.8 nm. This outcome suggests that the highest entanglement density in the plain weave imposes the most substantial constraint on the reptation of the strands, thereby preserving a relatively regular pore structure. In contrast, the absence of the primary peak and the appearance of a wide range of distribution of pores with various sizes are observed in both mix (2~3 nm) and basket weaves (1.5~3.5 nm), indicating considerable structural deformations.

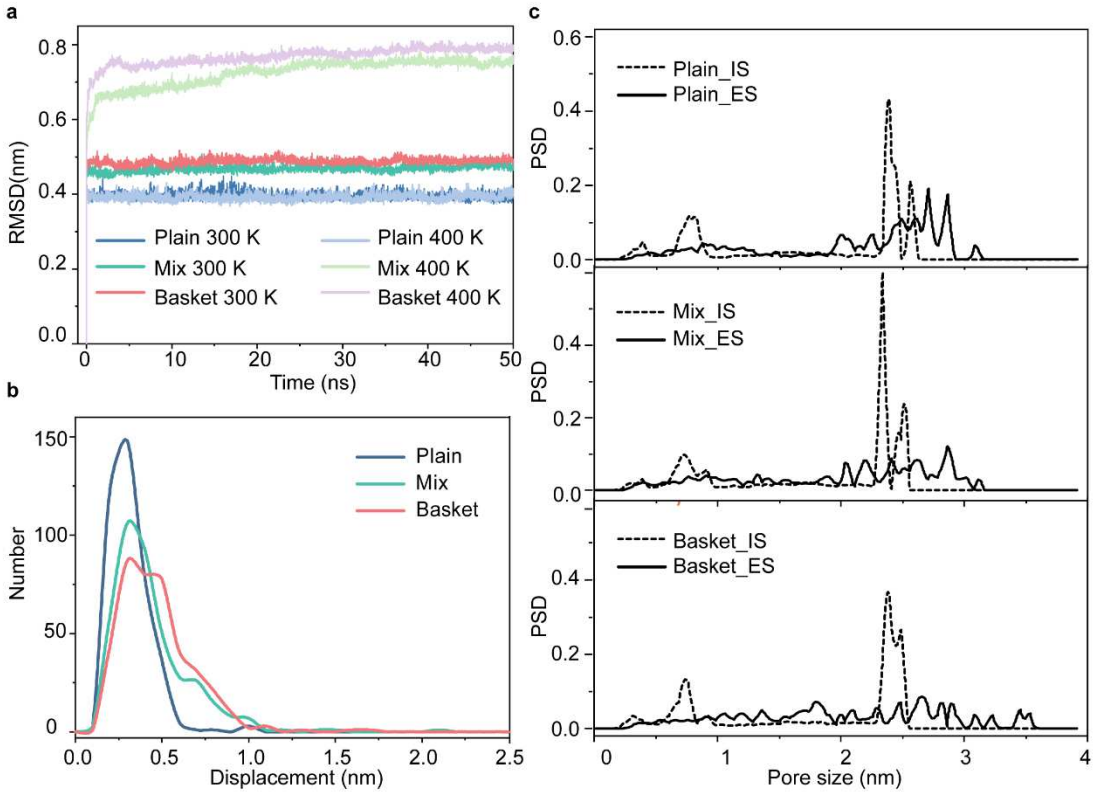


Fig. 2 | Analysis of stability of three weaves via equilibrium molecular dynamic (EMD) simulation. (**a**) Root-mean-square deviation (RMSD) analysis of three weaves at 300 K and 400 K

to assess their stability at equilibrium states (ES). The RMSD values for the 1/1 Plain weave are represented in navy and light blue at 300 K and 400 K, respectively; for the 2/1 Mix weave, they are depicted in dark and light green at both temperatures; and for the 2/2 Basket weave, they are coloured in pink and purple; the plain weave displays the least deformation across the temperature range, while for mix and basket weave, notably elevated RMSD values at higher temperatures suggest a progressive decrease in stability; (**b**) Distribution of crossing displacement (CD) across all 400 crossings in the three weaves from their initial models (IS) to equilibrium states (ES). Plain weave shows the narrowest CD distribution, while mix and basket feature a wider distribution, the results are in line with the RMSD simulation; (**c**) Pore size distribution analysis of the three weaves, illustrating the degree of spatial deformation between their initial and equilibrium states. IS are denoted by black dashed lines, while ES are represented by black solid lines. Three weaves exhibit similar pore distributions in their models. Upon reaching equilibrium, the plain weave demonstrates the least variation in the space field, evident from the presence of two peaks at 2.7 and 2.8 nm. These three simulation results indicate the relative stability of the weaves is related to their entanglement density and is as follows: 1/1 Plain weave, 2/1 Mix weave, and 2/2 Basket weave.

To provide a clearer understanding of the structural information contributing to the varying kinetic stability of the three weaves, the first-principles calculation in CP2K package[43] was carried out to optimize one of the repeating grids in three weaves. In the plain weave, three types of weft-wrap interactions were observed including the edge-to-face and face-to-face π-π interactions between aromatic TTZ units on weft and warp strands, and C-H···N hydrogen bonding between methyl hydrogen and the nitrogen atom on the benzimidazolylpyridyl unit (Fig. 3a). Calculations reveal that the face-to-face configuration has a 4.8 kcal/mol lower interaction energy compared to the edge-to-face configuration and the hydrogen-bond contributes ~3.4 kcal/mol interaction energy. Despite three weaves consist identical chemical composition, the change of weaving patterns varies both the type and strength of the interstrand interactions. Elaborately, while no discernible aromatic stacking alterations are observed in the mixed weave, there is a significant reduction in hydrogen bonding (5 pairs in plain weave *vs.* 1 pair in mixed weave), resulting in lower stability than that of the plain weave (Fig. 3b). Additionally, in the basket weave, we observe fewer face-to-face conformations (2 sets in both plain and mixed weaves *vs.* 1 set in basket weave), along with the absence of hydrogen bonding interactions within the grid, indicating the lowest stability (Fig. 3c). Conversely, the interlacing region lacks any significant weak interactions, resulting in a minimal contribution to the total energy. The simulation unequivocally illustrates the pivotal role of interstrand weak

interactions in stabilizing the weave, ensuring the strands retain their association within the material's pattern. Moreover, the strength of the weft-wrap interactions is directly correlated with the weaving pattern.

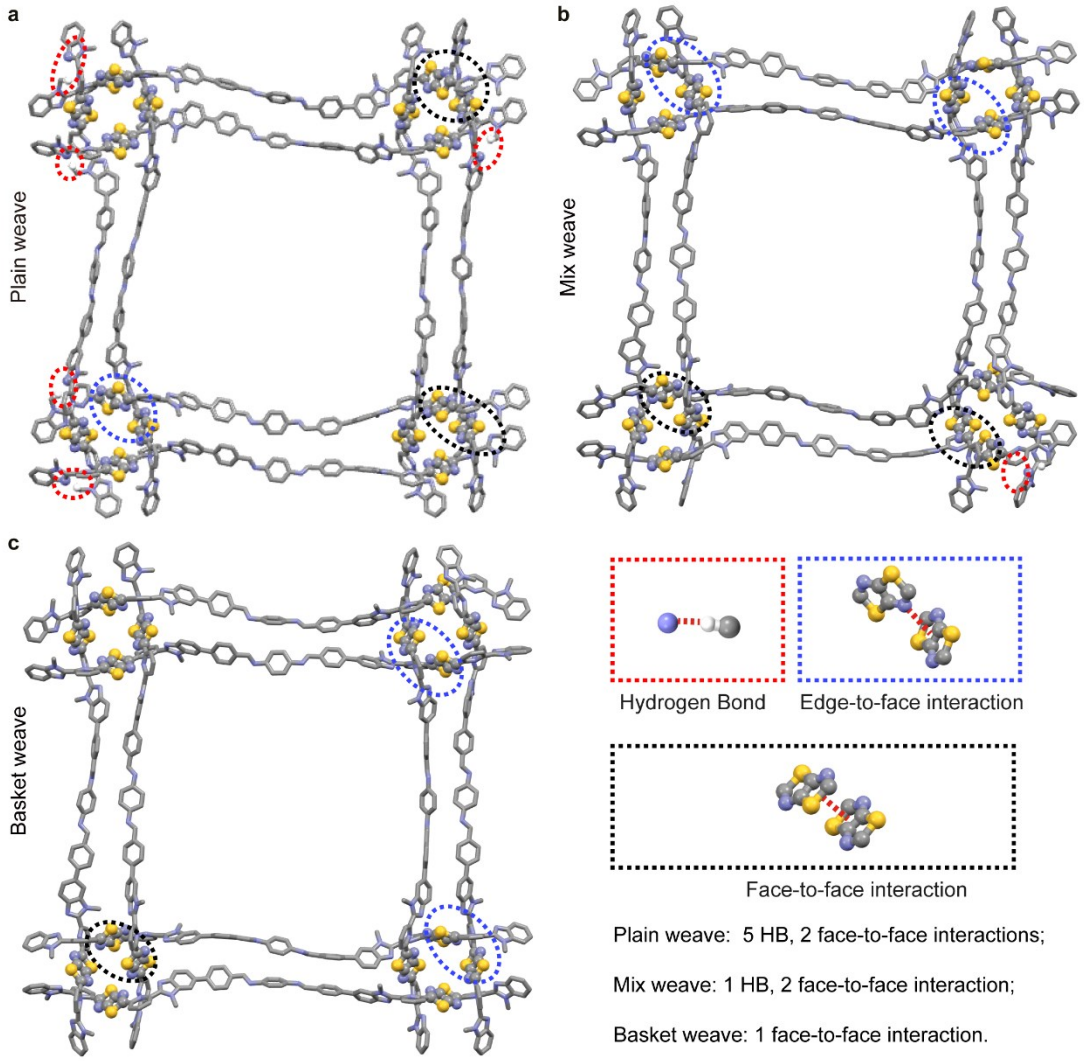


Fig. 3 | Interstrand non-covalent interactions analysis based on the optimized structures of the repeating grids in different weaves using first-principles calculations. Visualization of the interstrand non-covalent interactions including hydrogen bonding, face-to-face and edge-to-face π-π interactions of (**a**) 1/1 Plain weave; (**b**) 2/1 Mix weave; (**c**) 2/2 Basket weave. 2 sets of face-to-face π-π interactions along with 1 set of edge-to-face interaction and 5 pairs of C-H···N hydrogen bonds are found in the grid of 1/1 Plain weave, the binding energy of face-to-face interaction is 4.8 kcal/mol lower than the edge-to-face interaction whereas the hydrogen-bond contributes ~3.4 kcal/mol interaction energy. The grid of 2/1 Mix weave exhibits 1 pair of C-H···N hydrogen bonds and 2 sets of face-to-face π-π interactions which are not along a chain due to the lower entanglement density. In contrast, the repeating unit in 2/2 Basket weave has no C-H···N hydrogen bonding

interaction and only 1 set of face-to-face π-π interaction. The result demonstrates that the change of weaving pattern will significantly affect the interstrand interactions within the material networks, these interactions play the key role in stabilizing the weaves and influencing their kinetics, which are in agreement with the findings of their stability analysis.

As the entirely organic woven fabric represents a kinetically trapped high-energy state of ordered entanglements,[9] examining the local stress distribution and inter-strand interactions can yield valuable insights into its kinetics that are challenging to unveil through experimental methods. Subjecting the weaves to an NVT ensemble (canonical ensemble) at 300 K using the OPLS force field[44] gives the virial stress per atom[45]. Despite three weaves featuring different entanglement density, the mechanical stress at the contact field (the crossing regions) is notably higher than that of the free and interlacing fields (Fig. 4, Box 1a).

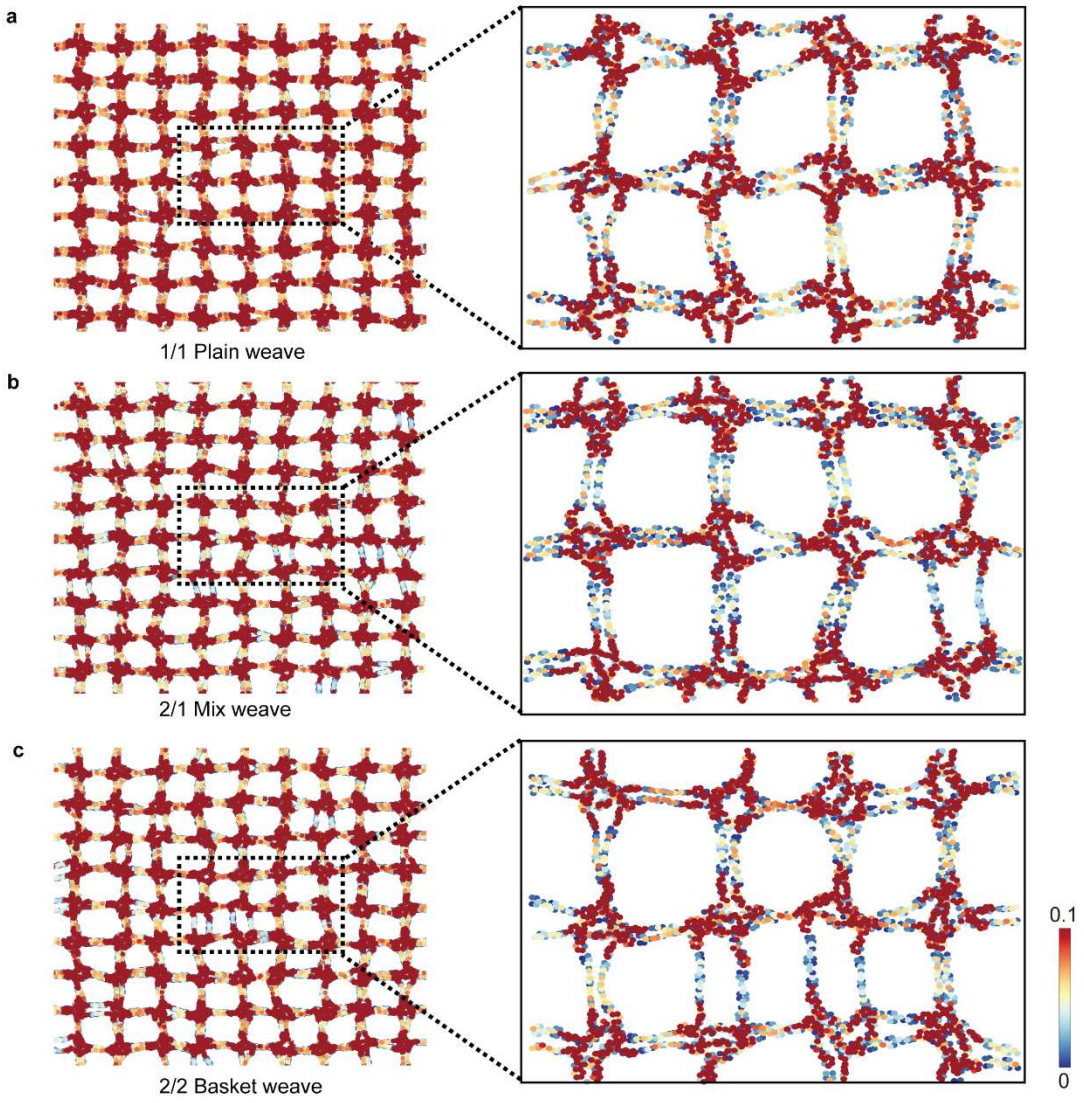


Fig. 4 | Normalized virial stress field comparison among three weaves. Visualization of the virial stress and a detailed zoom-in view of (**a**) 1/1 Plain weave; (**b**) 2/1 Mix weave; (**c**) 2/2 Basket weave. In all three weaves, regions of red signify higher mechanical stress whereas blue areas indicate lower stress levels. Despite the differences in the weaving patterns, mechanical stress is significantly higher at the contact field across all three weaves, particularly in the crossing regions, compared to the free and interlacing fields. The atomic stresses in the range of 0–3 bar have been normalized to a scale of 0 to 0.1 which allows for a clearer comparison of stress distributions at different regions, facilitating the identification of subtle variations in local stress profiles across the system

Mechanical performance of woven fabrics

Impact resistance of woven fabrics.

The significance of weaving architectures in determining the ballistic resistance and energy absorption process for macroscopic fabrics is widely acknowledged.[5,6] In order to explore the evolution of energy transfer during impact for molecular weaving polymers, we conducted a simulation of molecule-ballistic performance in a single-layer fabric structure using a non-penetrating impact model. For this simulation, we utilized a $7.3 \times 7.3 \times 5.5$ nm^3 iron cube as the projectile. Instead of employing critical velocity in macroscopic ballistic tests, we adjusted the contact pressures to the contact pressures at 0.3, 0.6, and 0.9 GPa (Fig. 5, Box 1c).

Variations in weaving patterns result in distinct stress distributions among the three weaves at identical pressures, and these distinctions amplify with increasing pressure. Notably, the plain weave, featuring the highest entanglement density, encounters substantially greater resistance while moving through the strands. Consequently, stress concentrates more prominently at the strands neighboring the impact center. With increasing pressure, the impact-induced chain sliding extended from the impact center to the far-field region of the weave, yet it did not reach the network boundaries. The minimal in-plane mechanical deformation in response to pressure indicates that thread-thread friction relaxation is the primary mechanism for energy dissipation in the plain weave. In contrast, the stress distribution in the basket weave appears to be the most dispersed among all three fabrics. This is due to the highest freedom of the strands, facilitated by the lowest entanglement density in the basket weave. Consequently, the cube can readily displace the strands away from its direction of travel to dissipate impact energy, resulting in considerable structural deformation compared to its initial configuration. The mixed weave, possessing a moderate number of entanglements, exhibits mechanical behavior resembling that of the plain weave at low pressure but akin to the basket weave

at high pressure. Both thread-thread friction relaxation and strand slippage play roles in dissipating energy in the mixed weave. The calculation of the crossing displacement (CD) profiles between ES and mechanical state (MS) further supported the observation (Supplementary Information, Figure S7). However, accurately quantifying the individual contributions of both pathways to the energy dissipation process remains challenging. Nevertheless, the findings highlight the significance of weaving pattern in determining the mechanical resistance of molecularly woven materials and the mechanism behind energy dissipation.

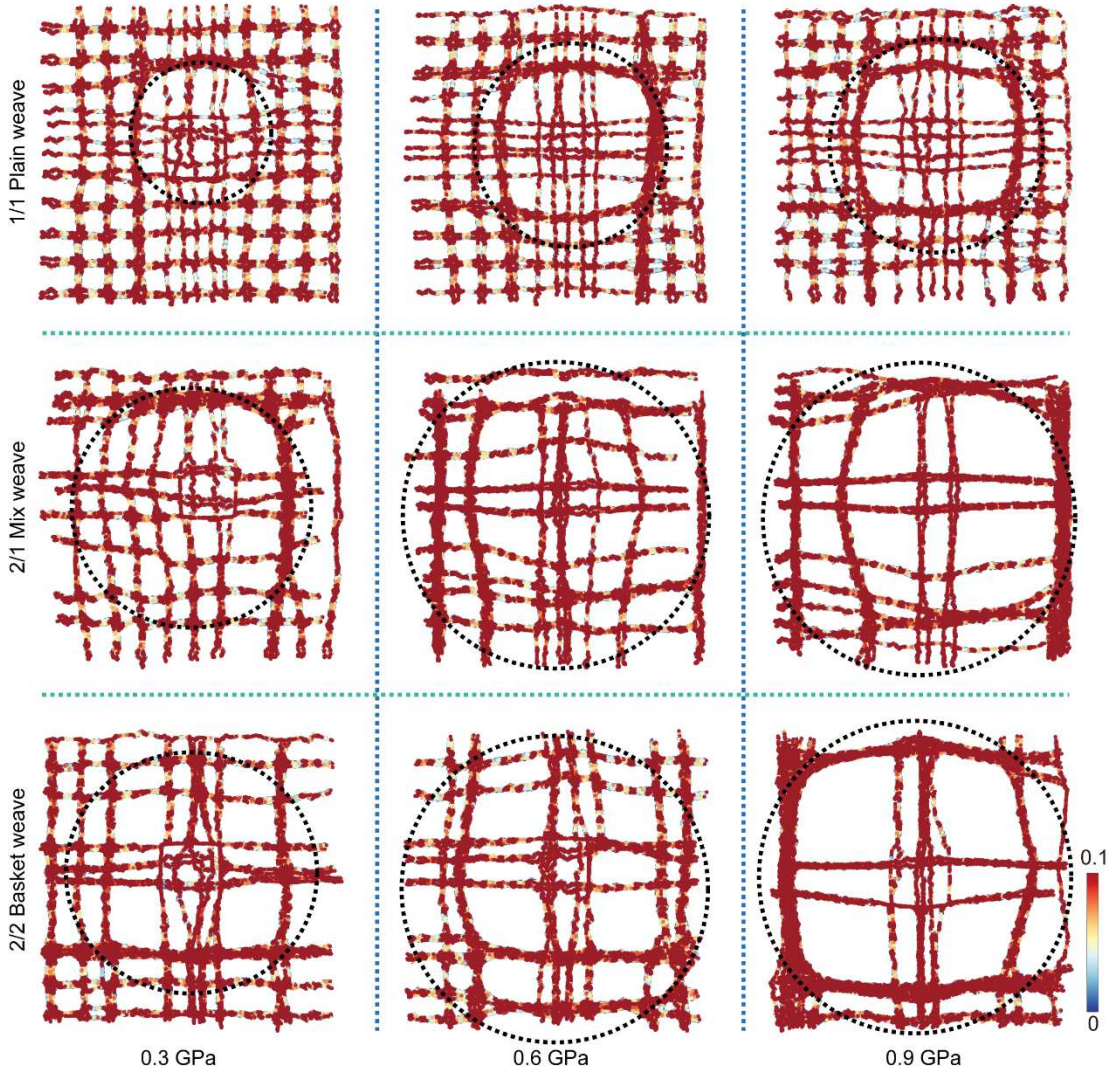


Fig. 5 | Mechanical response of three weave types under the different object intrusion. The simulation employs a non-penetrating impact model with a 7.3 × 7.3 × 5.5 nm^3 iron cube as the projectile, assessing molecule-ballistic performance in a single-layer fabric structure (including all 400 crossings). Normalized virial stress maps illustrate the response of the three weaves to the impact of the iron slab at pressures of 0.3, 0.6, and 0.9 GPa. The atomic stresses in the range of 0 – 3

bar have been normalized to a scale of 0 to 0.1 for a clearer comparison. Stress concentration is observed particularly at strands neighboring the impact centre. As pressure increases, impact-induced chain sliding propagates from the impact centre to the far-field region of the weave, without reaching the network boundaries. The plain weave encounters substantially greater resistance while moving through the strands. The mixed weave, possessing a moderate number of entanglements, exhibits mechanical behaviour resembling that of the plain weave at low pressure but akin to the basket weave at high pressure. The degree of deformation of the three weaves under various pressures can be categorized as follows: 1/1 plain weave < 2/1 mix weave < 2/2 basket weave.

Additionally, the free energy profile, as a function of strand displacement during the sliding process along with x (weft) direction, is calculated using the umbrella sampling method[46] to assess the kinetic barriers of various weaving architectures (Fig. 6). Notably, negligible energy changes occur when strand displacement is below 1 nm, indicating the strands can move freely in a short interval within the weaving network despite the existence of entanglements. However, a mechanical barrier emerges between 1.5 to 2.5 nm, as evidenced by a sharp increase in free energy across different weaves. Consistent with structural stability trends, the plain weave, with the highest entanglement density and strongest interstrand interactions, exhibits the highest energy barrier (34 kJ/mol) for strand sliding. Conversely, energy requirements for strand sliding decrease to 23 and 12 kJ/mol in mix and basket weaves, respectively. These discoveries emphasize that strands in weaves with lower entanglement density exhibit increased flexibility and reduced strand-strand friction, facilitating easier sliding within the network (Supplementary Information, Figure S8).

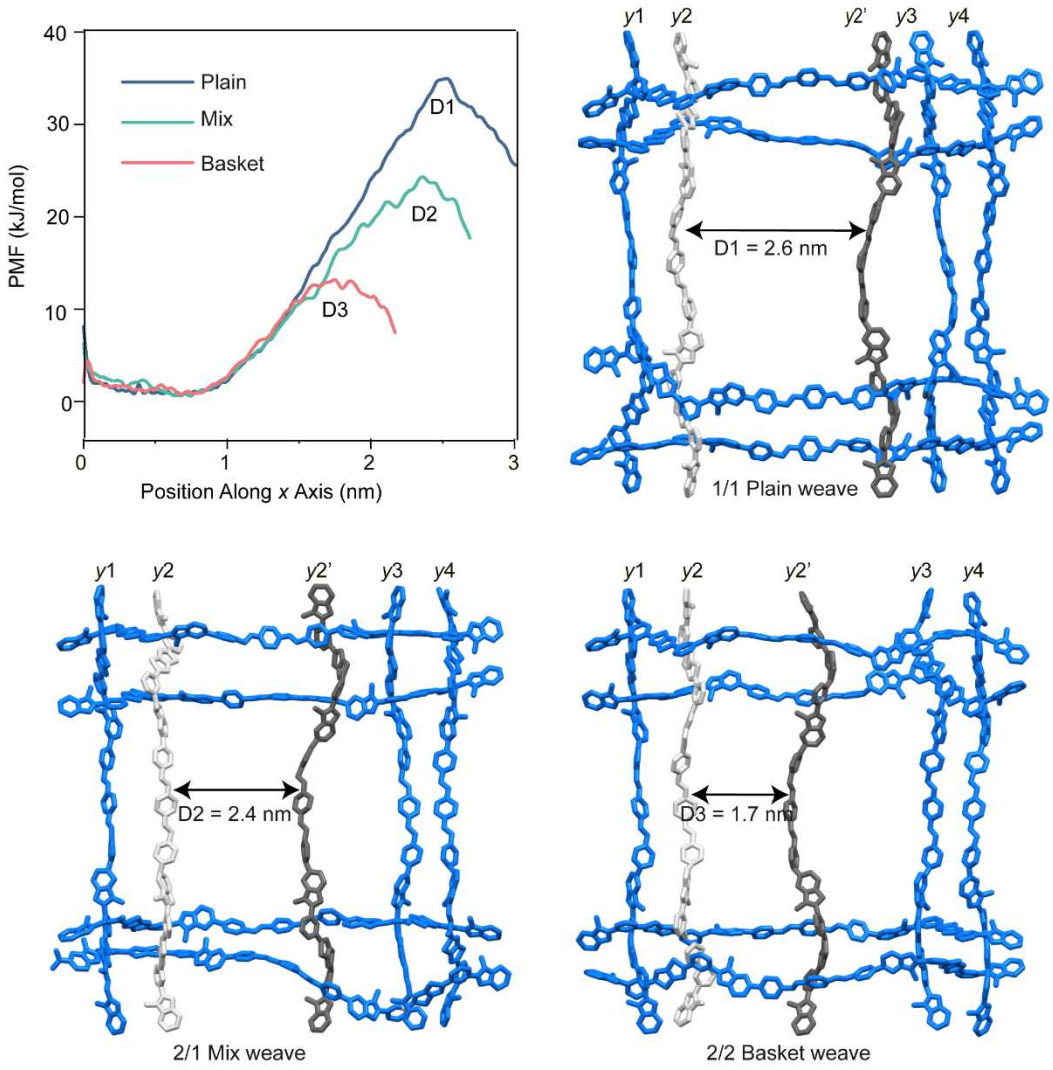


Fig. 6 | Energy analysis of strands pulling process in different weaves. The potential of mean force (PMF) analysis[47] was conducted on the pulling process of the selected polymer chain (*y*2) along the *x* direction in 1/1 Plain weave (navy), 2/1 Mix weave (green), and 2/2 Basket weave (pink). The initial position of *y*2 was depicted in light grey. Notable energy changes were observed when strand displacement was below 1 nm, indicating the ability of strands to move freely within the weaving network within a short interval despite entanglements. Mechanical barriers emerged between 1.5 to 2.5 nm, marked by a sharp increase in free energy across the different weaves. Consistent with structural stability trends, the plain weave exhibited the highest energy barrier (34 kJ/mol) when pulled along the *x* direction for 2.6 nm. In contrast, energy requirements for strand sliding decreased to 23 (by 2.4 nm displacement) and 12 kJ/mol (by 1.7 nm displacement) in the mix and basket weaves, respectively.

In-plane stretchability of woven fabrics.

In addition to the ballistic test, where force was applied vertically to the fabrics, the intra-ply stretchability[48] was explored using first-principles calculations (Supplementary Information, Figure S9). In contrast to macroscopic textiles that allow force to be applied to individual yarns, molecularly woven fabrics display a behavior where adjacent strands move in response when one strand is subjected to an external force. As a result, we performed in-plane tensile testing on the complete woven networks. The presence of the highest entanglement density in the plain weave has the lowest energy among the three optimized weaves without stretching. Before the strain ratio is up to 3%, the total energies of these woven patterns exhibit subtle change. When forces are further applied in both weft and warp directions, stretched strands prompt a significant rise in total energy (Box 1d). Certainly, the energy of the plain weave increases more rapidly than the other two weaves at the same strain ratio, indicating that the plain weave possesses the lowest flexibility due to its highest entanglement density. At a strain ratio of 9%, the total energy increase across the three weaves follows this ranking: plain weave (22.5 eV) > mix weave (22.1 eV) > basket weave (16.8 eV), correlating positively with the number and density of entanglements and interstrand interactions (Fig. 7a). The differential charge density (DCD) provides additional confirmation that the stretching-induced breakage of hydrogen bonds (C-H···N) and the weakening of aromatic π-π stacking collectively contribute to the stretchability of weave, evidenced by the shift of electron migration area from the interlacing field to the contact field (Fig. 7b). In contrast to the significant energy increase observed in the entire weaving structure (around 20 eV), the energy changes induced by stretching in free individual strands are 20-30 times lower (around 0.9 eV) (Fig. 7c). This substantial difference in energy disparity illustrates how the topology of woven structures can greatly reinforce the mechanical properties of individual molecular chains. (Corresponding changes of these weaves upon stretching at different ratios were illustrated in Supplementary Information, Figure S10-27) Additionally, during the stretching test, while the bond length in the free chain undergoes relatively uniform changes, in the weaves, it is concentrated in the entangled area (Supplementary Information, Figure S28). This observation again confirms that mechanical stress is primarily dissipated at the entanglements within the woven fabrics.

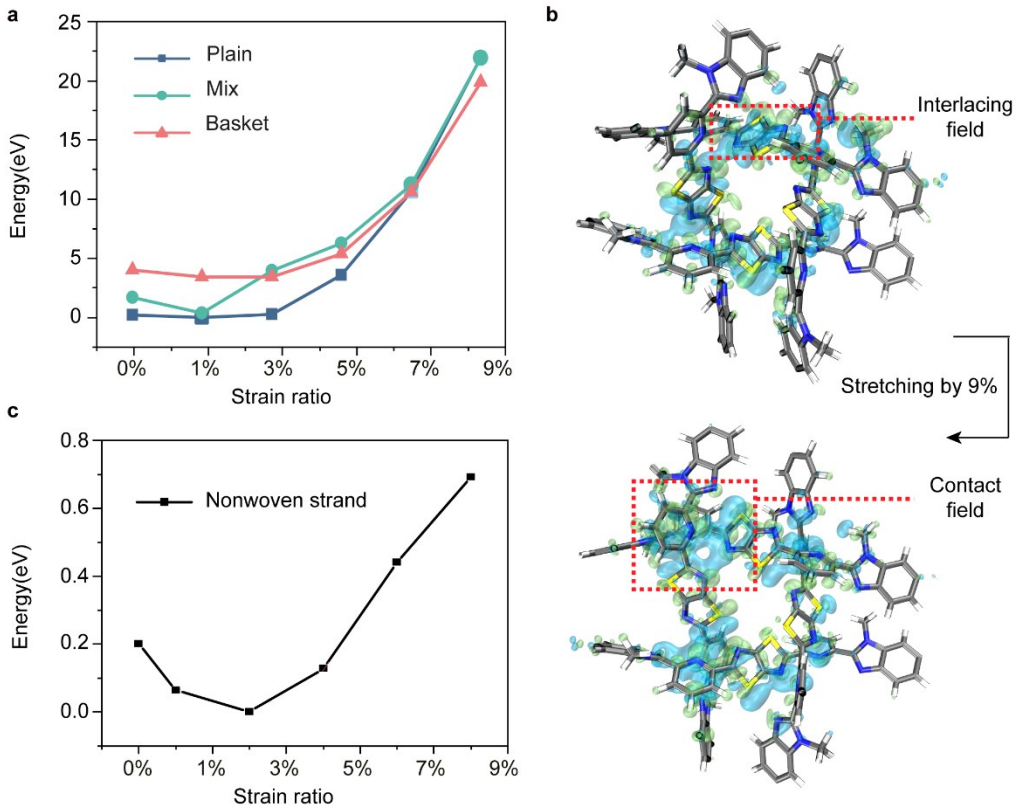
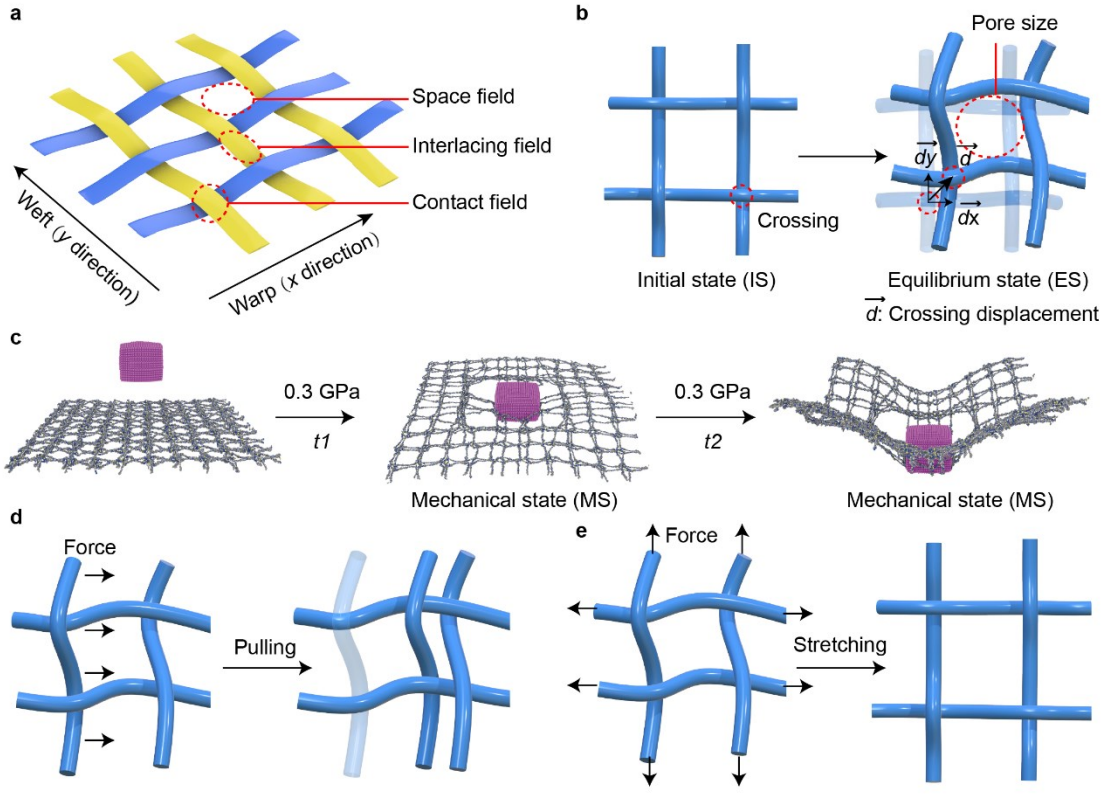


Fig. 7 | Total energy and charge density analysis of strands stretching process in different weaves using first-principles calculations. (**a**) Energy analysis of the stretching process on three weaves reveals distinct energy profiles. The plain weave (navy) exhibits a notably rapid increase in energy compared to the other two weaves at the same strain ratio, indicating its lowest flexibility due to the highest entanglement density and strongest interstrand weak interactions. Beyond a strain ratio of 1%, both the basket (pink) and mix weaves (green) demonstrate a similar energy trend. At a strain ratio of 9%, the strands reach a fully stretched conformation, with the total energy increase across the three weaves following this ranking: plain weave > mix weave > basket weave, reflecting a positive correlation with the number and density of entanglements and interstrand interactions; (**b**) Differential charge densities of contact field of plain weave in equilibrium state and strained by 9%. Shadow blue and green shades in the panels represent the loss and gain of electrons, respectively. Differential charge densities are visualized using isosurfaces of 0.0005 e/Bohr^3, it is noteworthy that electrons migrate from the interlacing field to the contact field upon stretching; (**c**) Energy analysis of a single strand in the stretching process shows significantly lower energy changes compared to the weaves. Stretching induces energy changes in free individual strands that are approximately 20-30 times lower, averaging around 0.9 eV.

Conclusion

Examining how weaving process and weaving patterns impact material properties at the molecular level is essential for designing and synthesizing woven and entangled polymers with enhanced physical and mechanical performance. Theoretical analysis of three distinct woven fabrics, all featuring the same molecular strands, reveals that weaving architectures play a pivotal role in shaping the dynamics, stability, and mesh structure of the weave. Additionally, the patterns influence the pathway of energy dissipation against external forces, directly affecting the mechanical behaviour of the materials. The effects stemming from weaving patterns can be attributed to the total number and density of entanglements and the interstrand non-covalent interactions, which physically restrict strand movement. This study not only establishes a clear correlation between weaving architectures and material characteristics but also presents a theoretical model capable of illustrating the implications of other weave's factors, such as strand rigidity and weave defects.[9,49]

Methods



Box 1 | Fabric field notations and schematic representation of different processes in this study. (**a**) Fabric field notations: Throughout the study, the weft (horizontal) direction is defined as the *x*-axis, and the warp (vertical) direction is represented by the *y*-axis. The space field refers to areas of the fabric where there is no direct interaction between warp and weft threads. The interlacing field describes the regions between two contact fields, while the contact field refers to the area where

weft and warp threads come into direct contact with each other. These factors contribute to the mechanical behaviour, strength, and stability of a weave; (**b**) Schematic representation of equilibrium process: A schematic representation of the equilibrium process of the repeat unit illustrates the differences between the initial state (IS) and the equilibrium state (ES). The pore represents the area of the space field between weft and warp threads, which can be utilized to trace changes in the weave between the initial and equilibrium state. '*d*' refers to the crossing displacement between the initial and equilibrium state; (**c**) Schematic illustration of the woven structure under different pressures: A schematic illustration depicts the alteration of a woven structure under varying pressures over time, revealing the deformation of the weave pattern as pressure increases; (**d**) Pulling process: In the pulling process, one of the wefts is selected to be pulled over with force. (**e**) Stretching process: The stretching process involves stretching the grid or object by applying force to both ends of the weft and warp threads.

Molecular Dynamic Simulations.

To gain a better understanding of its dynamic nature, three molecular weaves were simulated using all-atom molecular dynamic (MD) first in equilibrium molecular dynamic (EMD) and latter impact using a guest iron slab. Three molecular weaves were built in a cell with dimensions of 38 × 38 × 38 nm^3 using the Fortran code and parameterized within the OPLS forcefield,[44] while the particle mesh Ewald (PME) method was employed to calculate long-range electrostatic interactions. Both cutoff distances for the calculations were set at 10Å, which is shorter than half the length of the simulation cell. A time step of 2.0 fs was used, which could ensure good energy conservation. The system was simulated for 50 ns to equilibrate the weaving grids. The simulation utilized periodic boundary conditions, and a series system temperature of 300 K, 320 K, 340 K, 360 K, 380 K and 400 K was maintained for all weaving structures. To achieve this, V-rescale temperature coupling was employed to set the system in an NVT ensemble. After obtaining an equilibrium system, a non-equilibrium dynamic (NEMD) is performed for 20 ns to test the impact resistance of different weaving structures. A lump of iron impact on the weaving grids with a series fixed pressure 0.3, 0.6 and 0.9 GPa and the deformation can be observed. The trajectories were saved every 10 steps for further analysis. All simulations were performed by the GROMACS package.[50]

First-principles Calculations.

First-principles calculations were employed within the CP2K package,[43] utilizing a hybrid Gaussian plane wave (GPW) scheme. Wave function optimization was performed using matrix

diagonalization, and self-consistent field (SCF) convergence was achieved with the aid of Fermi smearing. The molecular orbitals of the valence electrons were expanded into DZVP-MOLOPT-SR-GTH basis sets, whereas the core electrons were described through Goedecker-Teter-Hutter (GTH)[51] pseudopotentials, and the energy cutoff for the plane wave expansion was set to 400 Ry. The exchange-correlation effects were described using the Perdew-Burke-Ernzerhof (PBE) functionals,[52] and dispersion corrections were applied using the Grimme D3 method[53] in all calculations. The single unit of weaving structures was comprised of 800 C atoms, 512 H atoms, 160 N atoms and 32 S atoms. All three weaving structures and single molecular chain were optimized in periodic boundary condition and strained by 1%, 3%, 5%, 7% and 9%. The dimensions of the simulation boxes are provided in Figure S9. Periodic boundary conditions are applied in the x-, y-, and z-directions for all calculations. In the electronic calculation, the differential charge density is defined as $\Delta\rho = \rho_{\text{total}} - \rho_{\text{weft}} - \rho_{\text{warp}}$, where ρ_{total} is the total charge density of weaving structures. ρ_{weft} and ρ_{warp} represent the charge density of weft and warp chains, respectively.

Statistical Analysis.

To identify the stability of different structures, this study characterized the root-mean-square deviation (RMSD) of the system, which can quantify differences in macromolecular structures and dynamics. given by the formula:

$$RMSD = \sqrt{\frac{1}{N}\sum_{i=1}^{N}\sigma_i^2} \quad (1)$$

where σ_i is the distance between atom i in the two frames, and N is the total number of equivalent atoms. Also, PSD function can reflect the deformation and quantify the distribution of diameters of a collection of spheres that best fill the pores in the simulated grids. To calculate the PSD, the Monte Carlo procedure was utilized.[54] The pore range of weaving structures was divided into small bins. A set of points were randomly placed in vacant domain (i.e., the space defined as the pores). For each point j, the porous space is probed to find the largest sphere that includes j and does not overlap the atom of the structures. After identifying the largest sphere, the bin value corresponding to its radius, along with those of all antecedent bins representing smaller radius, is augmented by one. The normalized bin distribution is in correspondence with the monotonically decreasing cumulative pore volume function $V_p(r)$, which is the volume of the pore space capable of being enclosed by spheres of radius r or smaller. The PSD is the derivation $\mathrm{d}V_p(r)/\mathrm{d}r$. In this work we screen weaving structures, mostly by using the PoreBlazer code developed for structural

characterization of porous materials.[42] Furthermore, the crossing point displacement is calculated to describe the slide of the polymer chains. We defined the mass centre of 10 closest pairs of atoms between two intersecting molecular chains as the crossing point. The distance between the mass centre in IS and ES is regarded as crossing point displacement. The schematic of definition of crossing point is provided in Figure S5.

The umbrella sampling (US) method[46] was used to calculate PMF for sliding of the molecular chains from the initial state to the deform state, where the sliding chain is kept straight. (a reasonable schematic is provided in Figure S8). All US simulations were 20 ns long, of which the initial 10 ns were discarded as equilibration. Umbrella potentials with a force constant of 5000 kJ mol^{-1}·nm^{-2} were applied to the chain center of mass and distributed with 0.2 nm spacing along the sliding direction. The pulling process of three architectures were presented in Figure S8. In all US calculations, positional restraints were unbiased using the weighted histogram analysis method (WHAM).[55]

To identity the simulated stress state in different weaving structures and impact condition, the virial stress per atom[45] $\boldsymbol{\sigma}$ has been characterized in this paper, given as:

$$\boldsymbol{\sigma} = \frac{1}{V}\langle \sum_{i=1}^{N} m_i \mathbf{v_i} \otimes \mathbf{v_i} + \mathbf{W}(\mathbf{r}^N) \rangle \quad (2)$$

where m_i and $\mathbf{v_i}$ are the mass and instantaneous velocity of the ith particle. The symbol $\otimes$ indicates the outer, dyadic, or direct tensor product. W is the global virial tensor, which depends only on the instantaneous atom positions $\mathbf{r}^N = \mathbf{r}_1, \mathbf{r}_2, \ldots, \mathbf{r}_N$ and the interactions between them. All the stress analysis was performed by a custom version of Gromacs,[56] implementing an algorithm for virial stress calculation.

Data availability

The authors declare that the main data supporting the findings of this study are available within the article and its Supplementary Information files. Extra data are available from the corresponding author upon request.

Code availability

The computational codes used in the current study are available from the corresponding author on reasonable request.

References

1 Cherenack, K. & van Pieterson, L. Smart textiles: challenges and opportunities. *J. Appl. Phys.* **112** (2012).

2 Ertekin, M., Ertekin, G. & Marmaralı, A. Analysis of thermal comfort properties of fabrics for protective applications. *J. Text. Inst.* **109**, 1091-1098 (2018).

3 Hu, J. & Xin, B. *Structure and mechanics of textile fibre assemblies* (Second Edition) (ed Peter Schwartz) 27-60 (Woodhead Publishing, 2008).

4 Grosberg, P. & Kedia, S. The mechanical properties of woven fabrics. *Text. Res. J.* **36**, 71-79 (1966).

5 Begum, M. S. & Milašius, R. Factors of weave estimation and the effect of weave structure on fabric properties: a review. *Fibers* **10** (2022).

6 Yang, C.-C., Tuan, N. & Phuong, T. Influences of weaving architectures on the impact resistance of multi-layer fabrics. *Mater. Des.* **85**, 282-295 (2015).

7 Scelzo, W. A., Backer, S. & Boyce, M. C. Mechanistic role of yarn and fabric structure in determining tear resistance of woven cloth: part I: understanding tongue tear. *Text. Res. J.* **64**, 291-304 (1994).

8 Shinohara, A., Shinohara, F. & Sakaebara, K. theoretical study on the anisotropy of the bending rigidity of woven fabrics. *J. Text. Mach. Soc. Jpn.* **32** (1979).

9 Zhang, Z.-H., Andreassen, B. J., August, D. P., Leigh, D. A. & Zhang, L. Molecular weaving. *Nat. Mater.* **21**, 275-283 (2022).

10 Liu, Y., O'Keeffe, M., Treacy, M. M. & Yaghi, O. M. The geometry of periodic knots, polycatenanes and weaving from a chemical perspective: a library for reticular chemistry. *Chem. Soc. Rev.* **47**, 4642-4664 (2018).

11 Herdlitschka, A., Lewandowski, B. & Wennemers, H. Organic molecular weaves. *Chimia* **73**, 450-454 (2019).

12 Liu, Y. & Yan, X. Woven polymer networks: from crystalline to elastomeric materials. *Chem. Eur. J.* **29** (2023).

13 Hubin, T. J. & Busch, D. H. Template routes to interlocked molecular structures and orderly molecular entanglements. *Coord. Chem. Rev.* **200**, 5-52 (2000).

14 Liu, Y. *et al.* Weaving of organic threads into a crystalline covalent organic framework. *Science* **351**, 365-369 (2016).

15 Xu, H.-S. *et al.* Single crystal of a one-dimensional metallo-covalent organic framework. *Nat. Commun.* **11**, 1434 (2020).

16 Xiao, D. *et al.* Single crystals of purely organic free-standing two-dimensional woven polymer networks. *Nat. Chem.* (2024).

17 Lewandowska, U. *et al.* A triaxial supramolecular weave. *Nat. Chem.* **9**, 1068-1072 (2017).

18 Li, G. *et al.* Woven polymer networks via the topological transformation of a [2]Catenane. *J. Am. Chem. Soc.* **142**, 14343-14349 (2020).

19 Guo, Y. *et al.* Synergistic covalent-and-supramolecular polymers with an interwoven topology. *ACS Appl. Mater. Interfaces.* **15**, 25161-25172 (2022).

20 Wang, Z. *et al.* Molecular weaving via surface-templated epitaxy of crystalline coordination networks. *Nat. Commun.* **8**, 14442 (2017).

21 August, D. P. *et al.* Self-assembly of a layered two-dimensional molecularly woven fabric.

Nature **588**, 429-435 (2020).

22 Ashbridge, Z. *et al.* Knotting matters: orderly molecular entanglements. *Chem. Soc. Rev.* **51**, 7779-7809 (2022).

23 Han, X. *et al.* Molecular weaving of chicken-wire covalent organic frameworks. *Chem* **9**, 2509-2517 (2023).

24 Zhang, Z.-H., Zhou, Q., Li, Z., Zhang, N. & Zhang, L. Completely stereospecific synthesis of a molecular cinquefoil (51) knot. *Chem* **9**, 847-858 (2023).

25 Feng, H.-N. *et al.* A star of David [2]catenane of single handedness. *Chem* **9**, 859-868 (2023).

26 Gao, W.-X., Feng, H.-J., Guo, B.-B., Lu, Y. & Jin, G.-X. Coordination-directed construction of molecular links. *Chem. Soc.* **120**, 6288-6325 (2020).

27 Liu, Y. *et al.* Molecular weaving of covalent organic frameworks for adaptive guest inclusion. *J. Am. Chem. Soc.* **140**, 16015-16019 (2018).

28 Neumann, S. E. *et al.* The propensity for covalent organic frameworks to template polymer entanglement. *Science* **383**, 1337-1343 (2024).

29 Saitta, A. M., Soper, P. D., Wasserman, E. & Klein, M. L. Influence of a knot on the strength of a polymer strand. *Nature* **399**, 46-48 (1999).

30 Liu, G., Rauscher, P. M., Rawe, B. W., Tranquilli, M. M. & Rowan, S. J. Polycatenanes: synthesis, characterization, and physical understanding. *Chem. Soc. Rev.* **51**, 4928-4948 (2022).

31 Kim, J., Zhang, G., Shi, M. & Suo, Z. Fracture, fatigue, and friction of polymers in which entanglements greatly outnumber cross-links. *Science* **374**, 212-216 (2021).

32 Ashton, P. R. *et al.* Supramolecular weaving. *Angew. Chem. Int. Ed. in Engl.* **36**, 735-739 (1997).

33 Huang, Q. *et al.* Dynamic molecular weaving in a two-dimensional hydrogen-bonded organic framework. *Chem* **7**, 1321-1332 (2021).

34 Everaers, R. *et al.* Rheology and microscopic topology of entangled polymeric liquids. *Science* **303**, 823-826 (2004).

35 Zhu, H., Tian, F., Sun, L., Wang, S. & Dai, L. Revisiting the non-monotonic dependence of polymer knotting probability on the bending stiffness. *Macromolecules* **54**, 1623-1630 (2021).

36 De Gennes, P. G. Reptation of a polymer chain in the presence of fixed obstacles. *J. Chem. Phys.* **55**, 572-579 (1971).

37 Edwards, S. F. & Vilgis, T. The effect of entanglements in rubber elasticity. *Polymer* **27**, 483-492 (1986).

38 Edwards, S. F. Statistical mechanics with topological constraints: I. *Proc. Phys. Soc.* **91**, 513 (1967).

39 Caraglio, M., Micheletti, C. & Orlandini, E. Stretching response of knotted and unknotted polymer chains. *Phys. Rev. Lett.* **115**, 188301 (2015).

40 Beves, J. E., Danon, J. J., Leigh, D. A., Lemonnier, J.-F. & Vitorica-Yrezabal, I. J. A solomon link through an interwoven molecular grid. *Angew. Chen. Int. Ed.* **54**, 7555-7559 (2015).

41 Zhao, Y. *et al.* A synthetic route for crystals of woven structures, uniform nanocrystals, and thin films of imine covalent organic frameworks. *J. Am. Chem. Soc.* **139**, 13166-13172 (2017).

42 Sarkisov, L., Bueno-Perez, R., Sutharson, M. & Fairen-Jimenez, D. Materials informatics with PoreBlazer v4.0 and the CSD MOF database. *Chem. Mater.* **32**, 9849-9867 (2020).

43 Kuehne, T. D. *et al.* CP2K: An electronic structure and molecular dynamics software package - Quickstep: Efficient and accurate electronic structure calculations. *J. Chem. Phys.* **152** (2020).

44 Jorgensen, W. L., Madura, J. D. & Swenson, C. J. Optimized intermolecular potential functions

for liquid hydrocarbons. *J. Am. Chem. Soc.* **106**, 6638-6646 (1984).

45 Thompson, A. P., Plimpton, S. J. & Mattson, W. General formulation of pressure and stress tensor for arbitrary many-body interaction potentials under periodic boundary conditions. *J. Chem. Phys.* **131** (2009).

46 Torrie, G. M. & Valleau, J. P. Nonphysical sampling distributions in Monte Carlo free-energy estimation: umbrella sampling. *J. Comput. Phys.* **23**, 187-199 (1977).

47 Roux, B. The calculation of the potential of mean force using computer simulations. *Comput. Phys. Commun.* **91**, 275-282 (1995).

48 Pegoretti, A., Fabbri, E., Migliaresi, C. & Pilati, F. Intraply and interply hybrid composites based on E-glass and poly(vinyl alcohol) woven fabrics: tensile and impact properties. *Polym. Int.* **53**, 1290-1297 (2004).

49 Orlandini, E., Baiesi, M. & Zonta, F. How local flexibility affects knot positioning in ring polymers. *Macromolecules* **49**, 4656-4662 (2016).

50 Pronk, S. *et al.* GROMACS 4.5: a high-throughput and highly parallel open source molecular simulation toolkit. *Bioinformatics* **29**, 845-854 (2013).

51 Goedecker, S., Teter, M. & Hutter, J. Separable dual-space Gaussian pseudopotentials. *Phys. Rev. B.* **54**, 1703-1710 (1996).

52 Perdew, J. P., Burke, K. & Ernzerhof, M. Generalized gradient approximation made simple. *Phys. Rev. Lett.* **78**, 1396-1396 (1997).

53 Grimme, S., Antony, J., Ehrlich, S. & Krieg, H. A consistent and accurate ab initio parametrization of density functional dispersion correction (DFT-D) for the 94 elements H-Pu. *J. Chem. Phys.* **132** (2010).

54 Sarkisov, L. & Harrison, A. Computational structure characterisation tools in application to ordered and disordered porous materials. *Mol. Simulat.* **37**, 1248-1257 (2011).

55 Kumar, S., Bouzida, D., Swendsen, R. H., Kollman, P. A. & Rosenberg, J. M. The weighted histogram analysis method for free-energy calculations on biomolecules. I. The method. *J. Comput. Chem.* **13**, 1011-1021 (1992).

56 Vanegas, J. M., Torres-Sanchez, A. & Arroyo, M. Importance of force decomposition for local stress calculations in biomembrane molecular simulations. *J. Chem. Theory Comput.* **10**, 691-702 (2014).

Acknowledgments

X.H. was supported by the National Natural Science Foundation of China (22273023), the National Key R&D Program of China (2019YFA0905200), Shanghai Municipal Natural Science Foundation (23ZR1418200), Natural Science Foundation of Chongqing (CSTB2023NSCQ-MSX0616), Shanghai Frontiers Science Center of Molecule Intelligent Syntheses, and the Fundamental Research Funds for the Central Universities. Z.-H.Z. thank National Natural Science Foundation of China (22301080). J.Y. thank National Natural Science Foundation of China (22203032). L.Z. thank National Natural Science Foundation of Shanghai (22ZR1479400), Natural Science Foundation of Chongqing (CSTB2023NSCQ-MSX0856), Frontiers Science Center of Molecular Intelligent Synthesis and East China Normal University for financial support. We also thank the Supercomputer

Center of East China Normal University (ECNU Multifunctional Platform for Innovation 001) for providing computer resources.

Author contributions

L.Z. and X.H. conceived the idea. Z.-H.Z. and Y.C. built up the weaving fabrics. S.C., Y.L. and J.Y. carried out the simulation. All authors contributed to data analysis and manuscript preparation. The project was directed by L.Z.

Competing interests

The authors declare no competing interests.

Additional Information

Additional information Supplementary information is available for this paper at xx. Correspondence and requests for materials should be addressed to L.Z.

ORCID IDs

Liang Zhang (0000-0001-8605-8681)

Xiao He (0000-0002-4199-8175)

Shiwei Chen (0009-0008-9307-643X)

Zhi-Hui Zhang (0000-0001-8927-1154)

Yuntao Li (0009-0005-4772-9012)

Yijing Chen (0000-0002-5865-6198)

Jinrong Yang (0000-0002-7678-0360)

Supplementary Files

This is a list of supplementary files associated with this preprint. Click to download.

- CoordinationSets.zip
- SupportingInformation.pdf